International Journal of Heat and Mass Transfer 52 (2009) 3613–3627

Contents lists available at ScienceDirect

International Journal of Heat and Mass Transfer

journal homepage: www.elsevier.com/locate/ijhmt

An experimental investigation of a mixed convection in a ⊔ shape channel subject to a reciprocating motion

Wu-Shung Fu *, Sin-Hong Lian, Ching-Lun Lin, Chung-Lin Yang

Department of Mechanical Engineering, National Chiao Tung University, 1001 Ta Hsueh Road, Hsinchu 30056, Taiwan, ROC

ARTICLE INFO

Article history:
Received 16 September 2008
Received in revised form 3 March 2009
Accepted 3 March 2009
Available online 4 May 2009

Keywords:
Experimental study
Mixed convection
Reciprocating motion

ABSTRACT

An experimental work is conducted to study heat transfer phenomena of a mixed convection in a ⊔ shape channel which is subject to a reciprocating motion. Simultaneously, a numerical calculation is executed to validate the experimental results auxiliarily. Parameters of Reynolds number, frequency and amplitude are considered. The results show that enhancement of heat transfer rate caused by the reciprocating motion is remarkable. Due to the impingement of cooling fluids, the heat transfer rate of the front heat region is still superior to those of the middle and back heat regions. The phenomena of this object are very complicated, and the maximum deviation between the experimental and numerical results is not over 25%.

1. Introduction

Protecting a piston from heat damage could effectively enhance the thermal efficiency of the heat engine and economize the usage of energy [1]. Lots of studies have been conducted to investigate similar objects recently.

Phenomena induced by a reciprocating straight channel which is somewhat similar to a reciprocating piston are interesting and have been widely investigated in the past. Grassma and Tuma [2] indicated that the mass transfer could achieve a level of about 2.5 times the stationary case. Patera and Mikic [3] showed that the above enhancement might result from flows mixing due to hydrodynamic instability induced by pulsating flows. The results of Kim et al. [4] were that the pulsating amplitude affected heat transfer significantly and a heat transfer impediment relative to the nonpulsating situation might occur in the thermally developing flow region. Nishimura [5–8] utilized a sinusoidal wavy-walled channel replacing a smooth duct to investigate heat transfer enhancement by pulsating and oscillatory flows numerically and experimentally. The results indicated that the higher heat transfer rates appeared as Reynolds numbers rose, and the flow patterns which affected heat transfer rates were directly influenced by the frequency of oscillatory remarkably. Chiu and Kuo [9] investigated turbulent heat transfer and predicted wall heat flux in a reciprocating engine by using an algebraic grid generation technique. The results showed that increasing the curvature of the cylinder head would increase the strength of induced squish flow and wall heat flux. Chang and Su [10] conducted an experimental work to investigate the influence of reciprocating motion on heat transfer inside a ribbed enclosure and showed that at the highest reciprocating speed, the heat transfer was enhanced about 145% of the equivalent stationary case. Chang and Su [1] modified the experiment and gained the results which at a pulsating number of 10.5, the time average Nusselt number could reach about 165% of the stationary one. Chang and Hung [11] developed a solution method for predicting unsteady flow and thermal fields in a reciprocating piston–cylinder assembly. The results showed that the two-stage pressure correction procedure could be readily incorporated into existing numerical techniques to yield reasonably accurate results. Sert and Beskok [12] studied oscillatory flow forced convection in micro-heat spreaders numerically. The results showed that a fluid with low viscosity, low density and high thermal conductivity was desired in coolant selection. Khaled and Vafai [13] considered the influence of fluids inertia and the effects of the presence of a magnetic field normal to the direction of the flow of an electrically conducting fluid on flow and heat transfer inside a nonisothermal and incompressible thin film undergoing oscillatory squeezing. It was found that the increment of the squeezing Reynolds number caused the flow instability to increase. Oppositely, the increment of the Hartmann number would lead the flow instability to decrease. The Nusselt number would be affected by the increasing squeezing Reynolds number. Afterward, Chang et al. [14] set an anti-gravity open thermosiphon system which was a more realistic model of a piston cooling system than the ones proposed before to study the heat transfer of a piston under the conditions in which cooling fluids flow through the piston channel. Effects of inertia,

* Corresponding author. Tel.: +886 3 5712121x55110; fax: +886 3 5720634.
E-mail addresses: wsfu@mail.nctu.edu.tw (W.-S. Fu), edenas.me94g@nctu.edu.tw (S.-H. Lian).

0017-9310/$ - see front matter © 2009 Elsevier Ltd. All rights reserved.
doi:10.1016/j.ijheatmasstransfer.2009.03.020

Nomenclature

A	area [m^2]
f_c	frequency [s^{-1}]
F_c	dimensionless frequency [$F_c = wf_c/v_0$]
Gr	Grashof number [$Gr = g\beta(T_w - T_\infty)w^3/\nu^2$]
h	heat transfer coefficient [W m^{-2} K^{-1}]
I	current [A]
k	thermal conductivity [W m^{-1} K^{-1}]
l	length of linking bar [m]
l_c	amplitude [m]
L_c	dimensionless amplitude [$L_c = l_c/w$]
$\overline{Nu}$	average Nusselt number (Eq. (4))
Q	heat energy [W]
Re	Reynolds number (Eq. (1))
ΔT_w	temperature difference [°C] ($\Delta T_w = T_w - T_\infty$)
v_c	velocity of reciprocating channel [m s^{-1}]
v_m	maximum velocity of reciprocating channel [m s^{-1}]
v_0	average velocity of air stream [m s^{-1}]
V	voltage [V]
w	width of channel [m]
Δy	thickness of basswood [m]

Greek symbols

ν	kinematics viscosity [m^2 s^{-1}]
τ	dimensionless time [$\tau = tv_0/w$]

Subscripts

b	basswood
h	heater
in	input
$loss$	loss

pulsating and buoyancy forces were taken into consideration and a correlation formula which was consistent with the heat transfer physics expressed with dimensionless temperature was proposed. Recently, Fu et al. [15] assumed a ⊓ shape channel as a piston to study a forced convection in the piston cooling system. The horizontal channel could move backward and forward periodically. Chang et al. [16,17] studied reciprocating thermosyphons fitted with transverse ribs and twisted tapes, respectively. The results showed that the heat transfer rates varied with inertia force, buoyancy force and pulsating number, and the heat transfer in the reciprocating thermosyphons were enhanced with fitted ribs and twisted tapes apparently. Besides, similar investigations of vibrational enclosure had been widely studied [18,19] in the past and systematically reviewed by Gershuni and Lyubimov [20]. Because the fluids could not flow into and out of the enclosure, the phenomena of the vibrational enclosure are quite different from those of the reciprocating channel. Limitation of the contents, the review and discussion of related studies of the vibrational enclosure are excluded.

However, the mechanisms of heat transfer taken into consideration in the stated literature were forced convection exclusively. Usually the temperature of the piston is very high, and the effect of natural convection on the heat transfer mechanisms should be considered for simulating more realistic situation. As a result, the object becomes a problem of a mixed flow in a ⊔ shape channel subject to a reciprocating motion. Since the heat surface is installed on the bottom side of the ⊔ shape channel and the directions of the gravity and inlet cooling fluids are downward which cause the phenomena of flow and thermal fluids to become complicated and interesting. Similar objects are seldom studied.

The aim of the study is mainly to investigate phenomena of a mixed flow in a ⊔ shape channel subject to a reciprocating motion experimentally. Numerical results obtained by the three-dimensional code of STAR-CD are used to authenticate the experimental results auxiliarily. The apparatus used in this study includes a cooling channel, reciprocating and heating control systems. Comparing both the experimental and numerical results, the maximum deviation between the experimental and numerical results is not over 25%.

2. Physical model and experimental procedure

A ⊔ shape cooling channel used in this study is shown in Fig. 1(a), and the related experimental apparatus which includes three main systems of a cooling channel system (5), a reciprocating system (4) and a heating control system (6 and 7).

In the cooling system, air streams flowing through the cooling channel (5) are sucked by a fan (1). The volume flow rate of air streams is measured by a flow meter (2) for calculating the average velocity of air streams used to compute a Reynolds number. For rectifying the air streams, a honey comb (3) is installed in the entrance of the cooling channel. The cooling channel is set vertically and composed of a reciprocating channel (51), two fixed channels (52) and two connecting channels (53). The reciprocating channel is set on the reciprocating system (4) to execute reciprocating motion.

In Fig. 1(b), the cooling channel is made of rectangular ducts of which the height and width are 120 mm and 30 mm, respectively. Lengths of each duct are shown in Fig. 1(b). The connecting channel (53) connects the reciprocating (51) and the fixed (52) channels. To avoid leakage of the air streams and improve the smoothness of reciprocating motion of the reciprocating channel, the tolerance among the connecting, reciprocating and fixed channels is filled with grease. Three heat regions of front, middle and back regions are sequentially arranged along the air streams flow, and the detailed dimensions are indicated in Fig. 1(c).

Shown in Fig. 2(a), the reciprocating system includes a stepping motor (41), a rotating circular plate (42), a linkage bar (43), a pedestal (44), a pair of tracks (45) and a pair of sliders (46). The stepping motor (41) installed below the pedestal (44) leads the rotating circular plate (42) to rotate, and via the linking bar (43) brings the sliders to move reciprocally. The rotating speed used for marine engine is slow, based on the information of Sulzer [21], the maximum frequency adopted in this work is 2/s. Since the reciprocating channel is set on the sliders shown in Fig. 2(b), the reciprocating channel can move with the sliders synchronously, and meets the demand of reciprocal motion.

In Fig. 2(c), the heat control system is composed of heat regions, thermocouples, temperature indicators and power supplies. Three heat regions of front, middle and back heat regions are set and each heat region includes five heaters. The main heater (712) of each region is adapted to measure heat transfer rate. The heat transfer rate of the mixed convection is small, and the prevention of the heat dissipation by a heat conduction mode from the main heater becomes important. Then the other four heaters ((711), (713), (714) and (715)) set around the main heater are used as guard heaters to prevent the heat dissipation from the main heater. In order to maintain a constant wall temperature condition on each heater, each heater is individually controlled by a power supply which is a direct current mode. As for the manufacturing of the heater, numerous small holes are drilled uniformly on a thin insulated

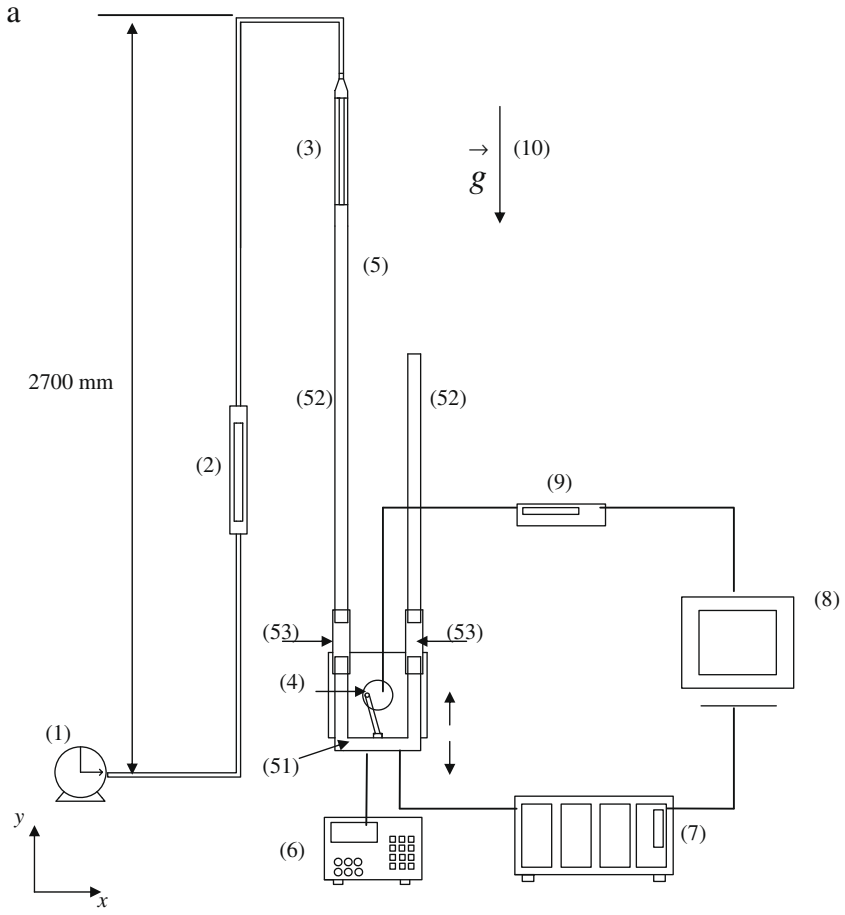

(1) fan
(2) flow meter
(3) honeycomb
(4) reciprocating system
(5) cooling channel
(51)reciprocating channel
(52)fixed channel
(53)connecting channel
(6)power supply
(7) temperature indicator
(8) personal computer
(9) motor driver
(10) direction of gravity

Fig. 1. (a) Experimental apparatus. (b) Dimensions of cooling channel. (c) Dimensions of each heat region.

material such as PCB (71), and a fine Ni–Cr line 0.1 mm (72) in diameter which is regarded as a heater during electrical power applying on threads through the holes tightly. A thin copper plate (74) covers the heater completely, and for prohibiting the copper plate to contact the Ni–Cr line directly, two thick pieces of Teflon tape (73) are separately interpreted into both places between the copper plate and heater. Three thermocouples (77) stuck on each copper plate are used to measure the temperature of the heater. Besides, a block of thin basswood (1.5 mm) is used to estimate heat dissipation by heat conduction from the bottom surface of the heater. Six thermocouples are then evenly installed on both surfaces of the thin basswood. A diameter of thermocouples is about 0.2 mm. Below the thin basswood, a block of thick basswood (6 mm) is set to prevent heat dissipation further.

As for flow visualization, a smoke–wire technique is adopted to observe variations of flow field qualitatively.

Each experiment data run includes three measurements and a brief outline is given as follows:

(1) The measurement of volume flow rate of air streams. Start the fan to blow air streams into the cooling channel system. Use the flow meter to read the magnitude of the volume flow rate $\dot{Q}$ of air streams, and the average velocity v_0 of the air streams could be obtained by dividing the volume flow rate by the cross-section area of the cooling channel. Sequentially Reynolds number Re of which the characteristic length w is 30 mm of the air streams is defined as the following equation:

$$Re = \frac{v_0 w}{\nu} \tag{1}$$

(2) The measurement of reciprocating movement. Select a designed revolution of the stepping motor which is a driving force for rotating circulating plate. Accompanying with the motion of the rotating circular plate, the linking bar moves around a circle continuously. As a result, the sliders brought by the linking bar move upwards and downwards circularly. The frequency and velocity of the reciprocating channel installed on the sliders could then be calculated.

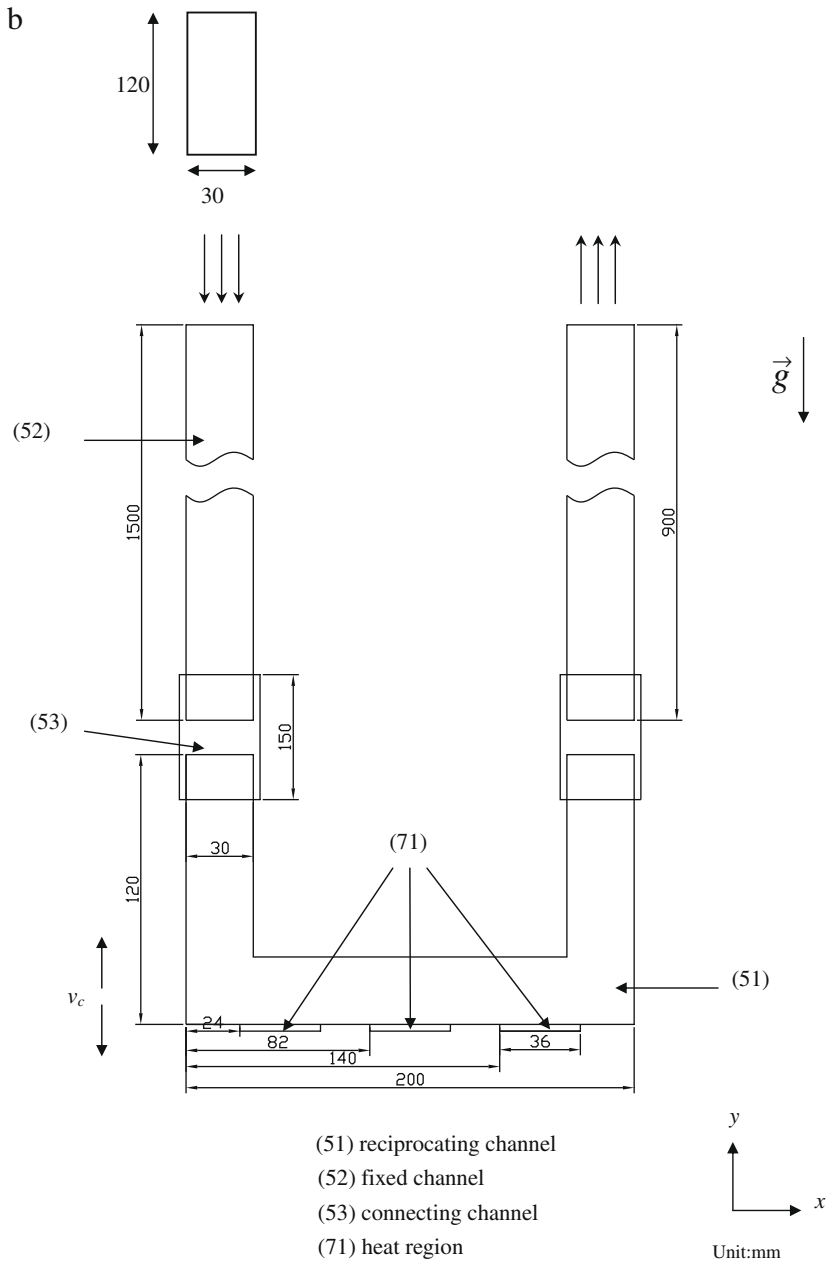

Fig. 1 (*continued*)

(3) The measurement of heat transfer rate of a heater. Electric power applies on each heater, and adjust amount of electric power of each heater carefully. Finally, the temperatures of each heater are close to a constant. The heat transfer rate of the main heat plate could be calculated by the following equation:

(a) Total input heat energy

$$Q_{in} = I \times V \tag{2}$$

where Q_{in} is the total input heat energy, I and V are current and voltage of electric power, respectively.

(b) Heat dissipation Q_{loss} from the basswood installed on the bottom side of the heater

$$Q_{loss} = k_b \times A_b \times \Delta T_b / \Delta y \tag{3}$$

where k_b is the thermal conductivity of basswood ($\fallingdotseq$0.055 W/(m K)), A_b is the area of basswood below the main heater, ΔT_b (°C) is the temperature difference between the upper and bottom sides of basswood and Δy is the thickness of basswood ($\fallingdotseq$1.5 mm).

(c) Calculation of the average Nusselt number $\overline{Nu}$ of the main heater

$$\overline{Nu} = \frac{hw}{k} = \frac{Q_{conv}}{A_h \cdot \Delta T_w} \cdot \frac{w}{k} \tag{4}$$

$$Q_{conv} = Q_{in} - Q_{loss} \tag{5}$$

where Q_{conv} is heat energy brought by the air stream flow, A_h is the area of heater, w is the width of cooling channel, ΔT_w (°C) is the temperature difference between the heater surface and environment. k is the thermal conductivity of air.

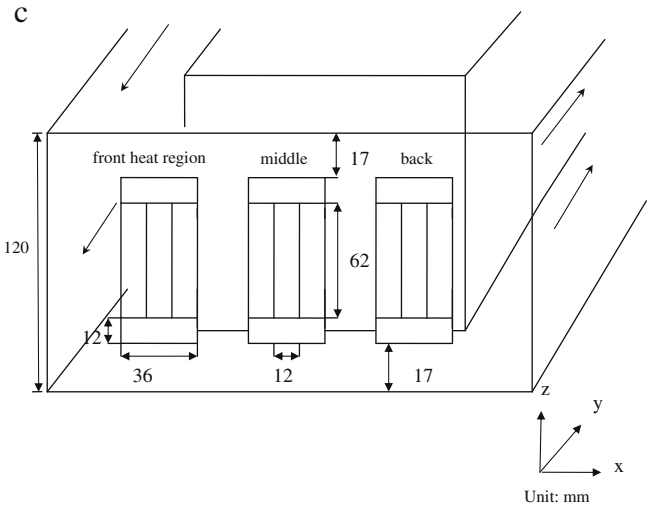

Fig. 1 (*continued*)

During the calculating processes, an average temperature of each thermocouple is used to calculate the heat transfer rate of each experimental run.

Based upon the measurements mentioned earlier, experimental procedures are briefly described as follows:

(1) Start the fan to provide a designed volume flow rate and calculate a corresponding Reynolds number.
(2) Turn on individual power supply to apply electric power Q_{in} to each heater.
(3) Adjust each power supply carefully until the temperature differences among the thermocouples installed on the heater surfaces are not over 0.3 °C.
(4) Acquire the necessary data to calculate the heat transfer rate of the main heater of each heat region for a stationary situation.
(5) Start the reciprocating system of which the amplitude is fixed and equal to 15 mm to obtain a selected frequency f_c.
(6) Acquire the necessary data to calculate the heat transfer rate of the main heater of each heat region for a selected reciprocating situation.
(7) Change the parameters of Re, f_c and Q_{in} to repeat the above procedures.

The situations conducted in this study are indicated in Table 1. According to the data of makers, the resolutions of the thermocouples and temperature instruments are 0.75% and 0.1 °C, respectively. The uncertainty analyses are based on Kline [22], and the magnitudes of uncertainty of the related parameters of different Reynolds numbers are tabulated in Tables 2 and 3.

For validating the experimental results, a numerical method is executed auxiliarily. Corresponding to the main part of experimental apparatus, a three-dimensional physical model is simulated, and 1% turbulence intensity at the inlet are adopted for the k–ε model. In calculating processes, finite volume methods are used to discretize the equations of Nabier–Stokes, energy and k–ε model. The results of steady and transient states are resolved by the methods of SIMPLE and PISO, respectively, and total grids of 597,335 are used. As for the treatment of reciprocating motion, a method of the elongation and contraction of the grids distributed in the reciprocating motion zone which is the same as the one developed in the authors' previous study [15] is used. The boundary conditions of reciprocating zone are slip condition and consistent with the reciprocating motion. A condition of constant temperature is assigned on the heat regions, and the other regions are insulated condition.

3. Results and discussion

Due to the limitation of the apparatus, the dimensionless amplitude L_c is selected and equals to 0.5. The dimensionless velocity V_c of the reciprocating system used in the numerical method is defined as the following equation:

$$V_c = \frac{v_c}{v_0} = 2\pi F_c L_c \cos(2\pi F_c \tau) \tag{6}$$

In this study, the real distance from the shaft of stepping motor to the slider is s shown in Fig. 3, and could be expressed as the following equation:

$$S = \frac{s}{w} = L_c \sin(2\pi F_c \tau) - \sqrt{L^2 - (L_c \cos(2\pi F_c \tau))^2} \tag{7}$$

Differentiate S by time τ, and the velocity V_c of the slider could be calculated and is expressed as the following equation:

$$V_c = \frac{v_c}{v_0} = 2\pi F_c L_c \cos(2\pi F_c \tau) - 2\pi F_c L_c^2 \frac{\cos(2\pi F_c \tau)\sin(2\pi F_c \tau)}{\sqrt{L^2 - (L_c \cos(2\pi F_c \tau))^2}} \tag{8}$$

The velocity deviations between the experimental and numerical velocities are existent because of the ratio of (l/l_c) and shown in Fig. 3. According to the apparatus size, the ratio of (l/l_c) used in this study is 3.53. The deviation between both velocities is slight, and both velocities are approximately equivalent.

Photographs of the visualization are shown in Fig. 4. White lines indicate the positions of fine metal lines set in the reciprocating channel. To apply paraffin on the lines and turn on electrical power, white smoke which illustrates the conditions of flow fields will be produced from the lines immediately. The positions of thick solid lines indicated in the numerical result virtually simulate the corresponding positions of fine metal lines shown in Fig. 4, and the thin solid lines in the same figure represent the streamlines of main stream flows obtained by the numerical method mentioned above. Fig. 4(a) and (b) are at the stationary state of $Re = 150$ and $\Delta T_w = 40$ °C situation, and Fig. 4(c) and (d) are at an instant of the reciprocating state of $Re = 150$, $\Delta T_w = 40$ °C, $F_c = 0.2$ and $\tau = \frac{3}{4}\tau_p$ situation. At the stationary state shown in Fig. 4(a) the main stream flows are not interrupted by a reciprocating motion, the main stream flows gather together and form a drain, and a small circulation zone is accessorily formed in the left corner. These phenomena are clearly indicated in the part (2) of Fig. 4(a). However, the white smoke produced by the paraffin is easily dispersed by the main stream flows along the region of drain and it has difficult to remain the traces of white smoke. In the corner of drain, the white smoke indicating the main stream flows cannot be observed. Oppositely, in the circulation zone the fluids are stagnant that causes the traces of white smoke to be remained easily, then the white smoke can be observes in the left corner and shown in the part (1) of Fig. 4(a). In Fig. 4(b), in the outlet region the drain of the main stream flows is somewhat enlarged relative to that in the inlet region. Then the traces of main stream flows indicated by the white smoke are chased in the part (1) of Fig. 4(b). The circulation zone is as usual found in the right corner. Under reciprocating states of Fig 4(c) and (d), the main stream flows are interrupted by the reciprocating motion, then the traces of main stream flows are more easily chased relative to those at the stationary state. The results of experimental works and numerical calculations are consistent qualitatively in the above figures that can validate the phenomena of the experimental works to be creditable.

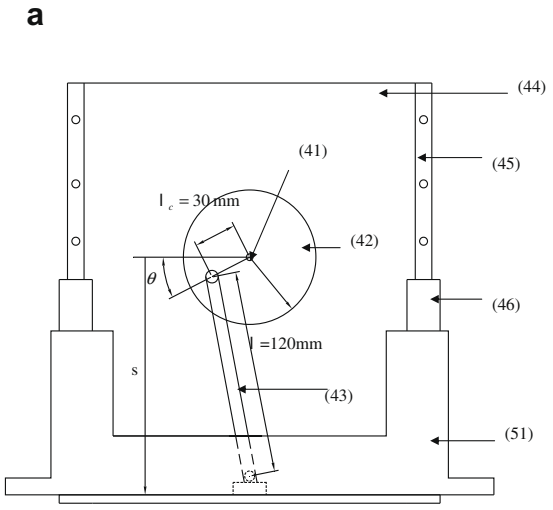

(41) motor transmission shaft
(42) rotating circular plate
(43) linking bar
(44) pedestal
(45) track
(46) slider
(51) reciprocating channel

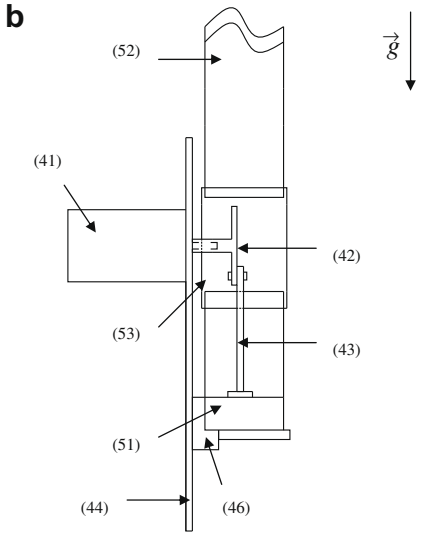

(41)stepping motor
(42)rotating circular plate
(43)linking bar
(44)pedestal
(46)slider
(51)reciprocating channel
(52)fixed channel
(53)connecting channel

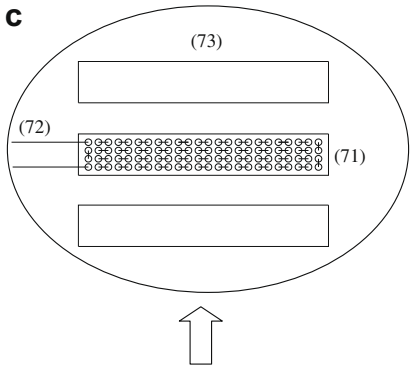

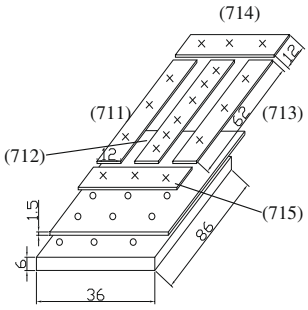

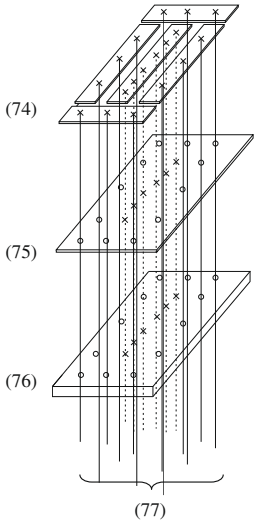

(71) heater
(72) Nickel-Chromium alloy wire
(73) Teflon tape
(74) thin cooper plate
(75) 1.5mm basswood
(76) 6mm basswood
(77) thermocouples
(711) guard heater
(712) main heater
(713) guard heater
(714) guard heater
(715) guard heater

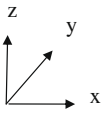

unit:mm

Fig. 2. (a) A reciprocating system. (b) A combination of cooling channel system and reciprocating system. (c) Hater structure.

Table 1
Parameters conducted in experimental runs.

	Re	Gr/Re^2	ΔT_w (°C)	F_c	L_c	v_c/v_o
Case1	300	0.40	10	0.0	0.0	0.0
Case2	300	0.81	20	0.0	0.0	0.0
Case3	300	1.21	30	0.0	0.0	0.0
Case4	300	1.62	40	0.0	0.0	0.0
Case5	200	0.91	10	0.0	0.0	0.0
Case6	200	1.82	20	0.0	0.0	0.0
Case7	200	2.73	30	0.0	0.0	0.0
Case8	200	3.64	40	0.0	0.0	0.0
Case9	150	1.62	10	0.0	0.0	0.0
Case10	150	3.24	20	0.0	0.0	0.0
Case11	150	4.85	30	0.0	0.0	0.0
Case12	150	6.47	40	0.0	0.0	0.0
Case13	300	0.40	10	0.2	1.0	1.26
Case14	300	1.62	40	0.2	1.0	1.26
Case15	300	0.40	10	0.4	1.0	2.51
Case16	300	1.62	40	0.4	1.0	2.51
Case17	200	0.91	10	0.2	1.0	1.26
Case18	200	3.64	40	0.2	1.0	1.26
Case19	200	0.91	10	0.4	1.0	2.51
Case20	200	3.64	40	0.4	1.0	2.51
Case21	150	1.62	10	0.2	1.0	1.26
Case22	150	6.47	40	0.2	1.0	1.26
Case23	150	1.62	10	0.4	1.0	2.51
Case24	150	6.47	40	0.4	1.0	2.51

Table 2
Uncertainty analyses of front heat region under Re = 300.

Parameters	Dimensions	Uncertainty
w (mm)	30 mm	0.05 (mm)
ΔT_W (°C)	20 °C	±0.3(°C)
L_c	15 mm	±0.11%
Re	300	±1.78%
$\overline{Nu}$	7.96	±1.89%
Gr/Re^2	0.81	±3.88%

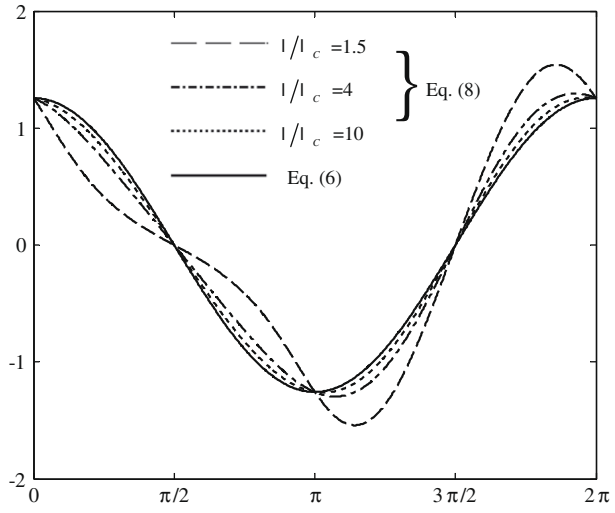

Fig. 3. Velocities of reciprocating channel.

In order to prove the reliability of the apparatus, the apparatus at the stationary and reciprocating situations under the same condition are conducted three times, respectively. In Fig. 5(a) and (b), the results of both situations are consistent well, and the maximum deviations are not over 5%. The functions and stability of this apparatus are credible.

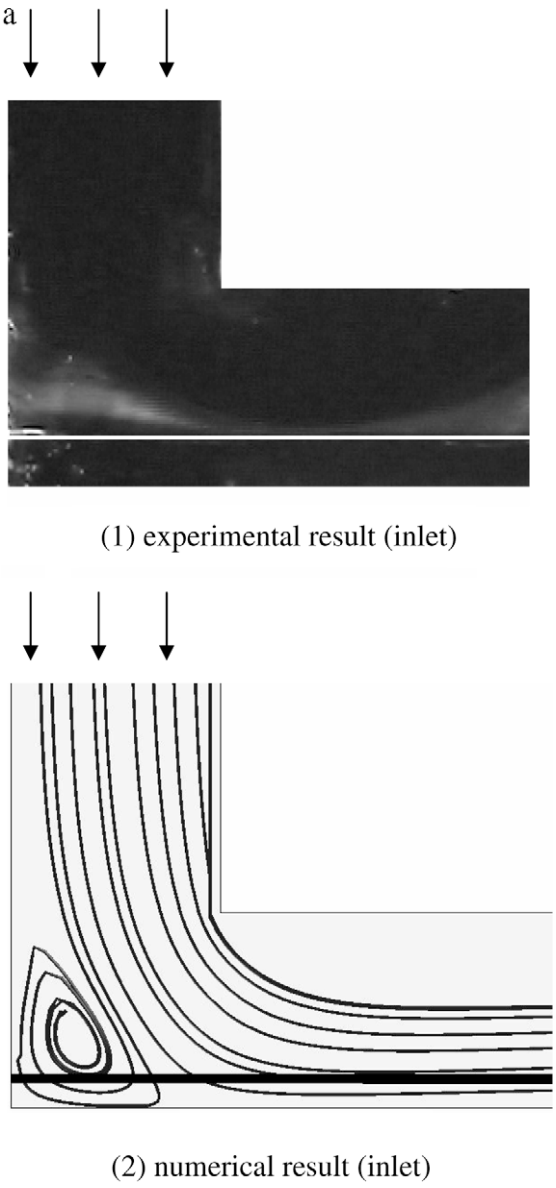

Fig. 4. (a) A stationary state for Re = 150, ΔT_w = 40 °C. (b) A stationary state for Re = 150, ΔT_w = 40 °C. (c) A reciprocating state for Re = 150, ΔT_w = 40 °C. (d) A reciprocating state for Re = 150, ΔT_w = 40 °C.

The maximum reciprocating velocity v_m and the mean velocity of inlet fluid v_0 are tabulated in Table 4. In Fig. 6, the results of different frequencies under Re = 300, ΔT_w = 10 °C and L_c = 0.5 are indicated. The solid and hollow signs represent the experimental and numerical results, respectively, and the maximum deviation between both results is about 20%. In this study, three heat regions are separately distributed in the bottom wall, the main stream flow of which the strength is controlled by Reynolds number flows over the whole region and the effect of the Gr/Re^2 on the flow is only around the heat region. The front heat region is subject to the impingement of cooling fluids, the Nusselt numbers of the front heat region are then larger than those of the middle and back heat regions apparently for each frequency situation. The flow flows over the middle heat region to be similar to a channel flow because the flow is confined by the top and bottom walls of the reciprocating channel. The direction of the reciprocating motion of the channel is vertical to that of the main stream flow. As a result, the contribution of the frequency F_c to the heat transfer rate of the

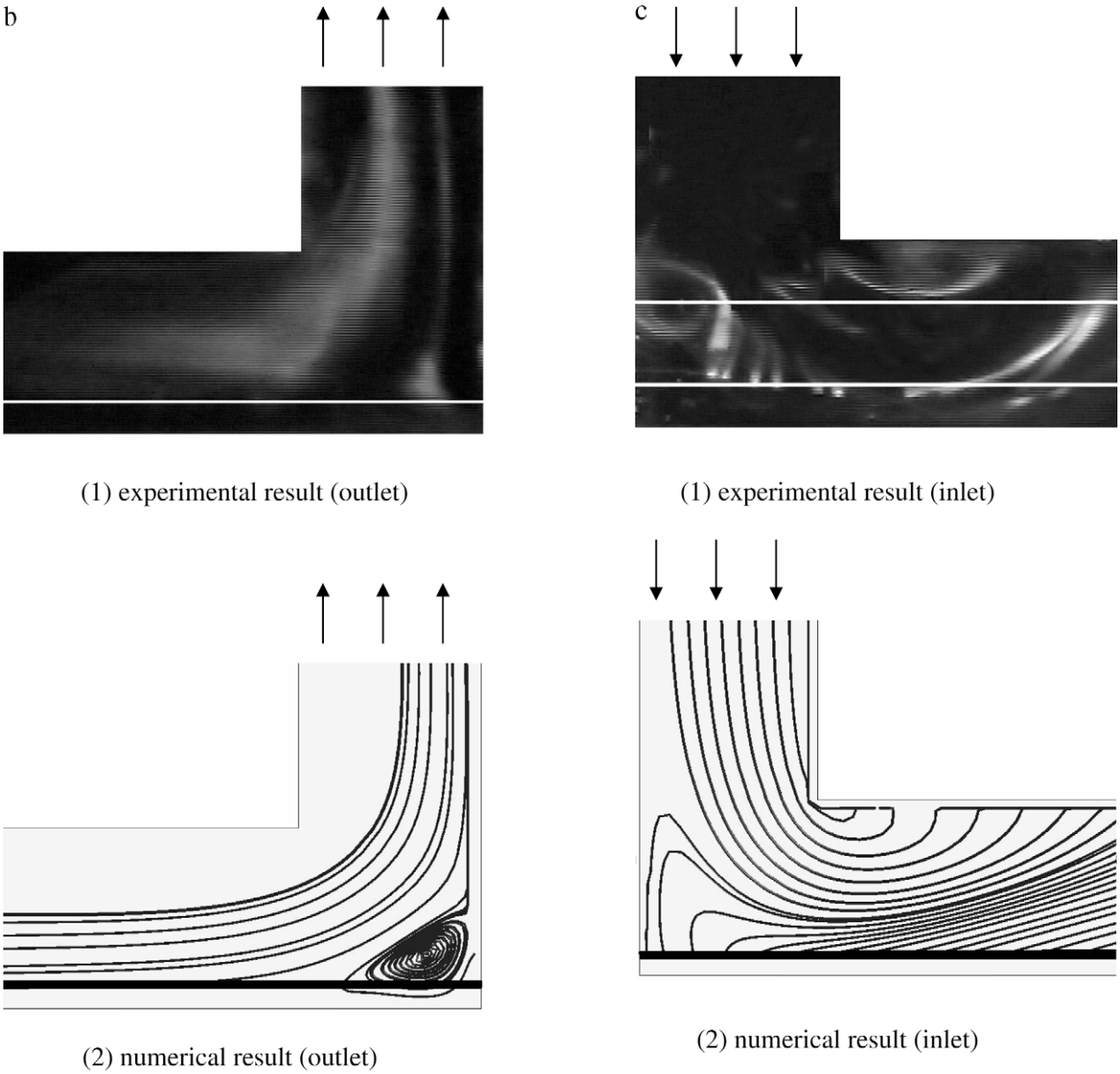

Fig. 4 (*continued*)

middle heat region weakens and the average Nusselt numbers of the frequencies of 0.2 and 0.4 are almost equivalent and shown in Fig. 6(b).

The back heat region is installed near the right corner of the bottom wall. And the main stream flow direction turns from horizontal to upward in this corner. The higher the frequency is, the flow turns round the corner more quickly and has difficulty to flow over the back heat region completely. Therefore, the contribution of the frequency to the heat transfer rate cannot be corresponding to the expectation of a higher frequency gaining a larger Nusselt number in the back heat region. Shown in Fig. 6(c), the average Nusselt number of $F_c = 0.4$ situation is not larger than that of $F_c = 0.2$ situation. But the difference between both average Nusselt numbers is not remarkable.

The Nusselt numbers of the heat regions under the reciprocating motions ($F_c = 0.2$ and 0.4) are generally larger than those of the heat regions under no reciprocating motion ($F_c = 0.0$) situation. The enhancement caused by the reciprocating motion is effective. In this figure, the magnitude of the Gr/Re^2 is about 0.40, and the dominance slightly inclines to a forced convection. Then the variations of the magnitudes of average Nusselt numbers are from large to small along the direction of main stream flow and the trend is similar to that of Fu et al. [15].

In Fig. 7, the temperature difference ΔT_w increases to 40 °C, and the magnitude of Gr/Re^2 becomes 1.62. The influence of natural convection increases. The Nusselt numbers on the front and back heat regions of this situation are larger than those on the front and back heat regions shown in the above figures (Fig. 6(a) and (c)). However, in the middle heat region because of confinement of the top and bottom walls of the reciprocating channel the influence of the natural convection is not apparent, and the magnitudes of Nusselt numbers on this region are close to those shown in Fig. 6(b).

Shown in Fig. 8, the magnitude of Reynolds number is 200, and the influence of the forced convection becomes weaker than the situation shown in Fig. 6. As a result, all the magnitudes of Nusselt numbers in the front, middle and back heat regions in this situation are smaller than those indicated in the corresponding regions

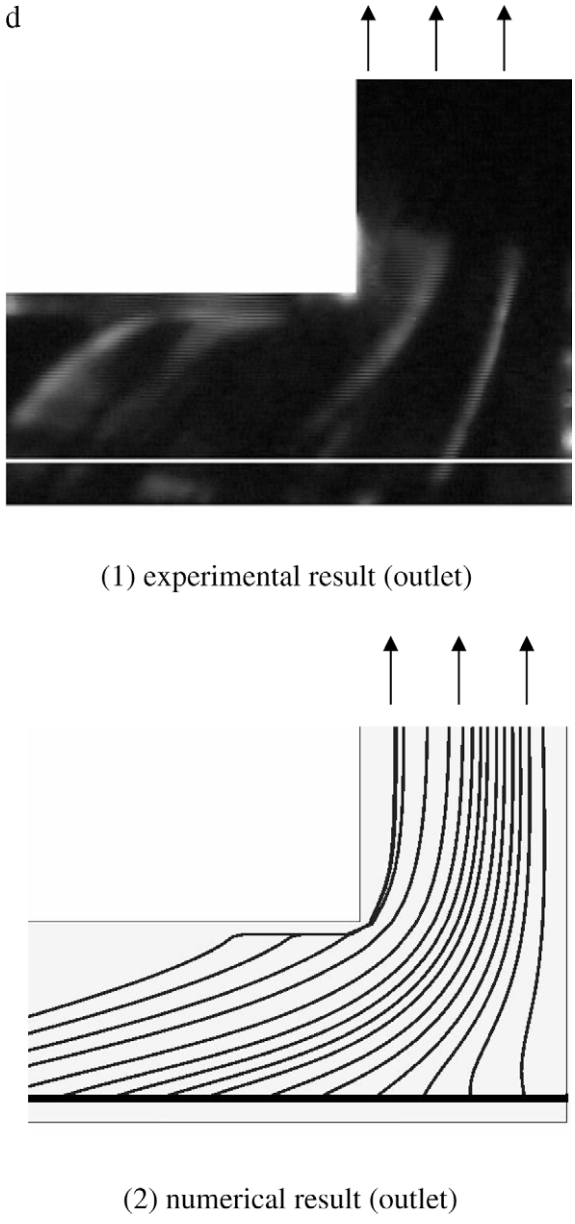

Fig. 4 (*continued*)

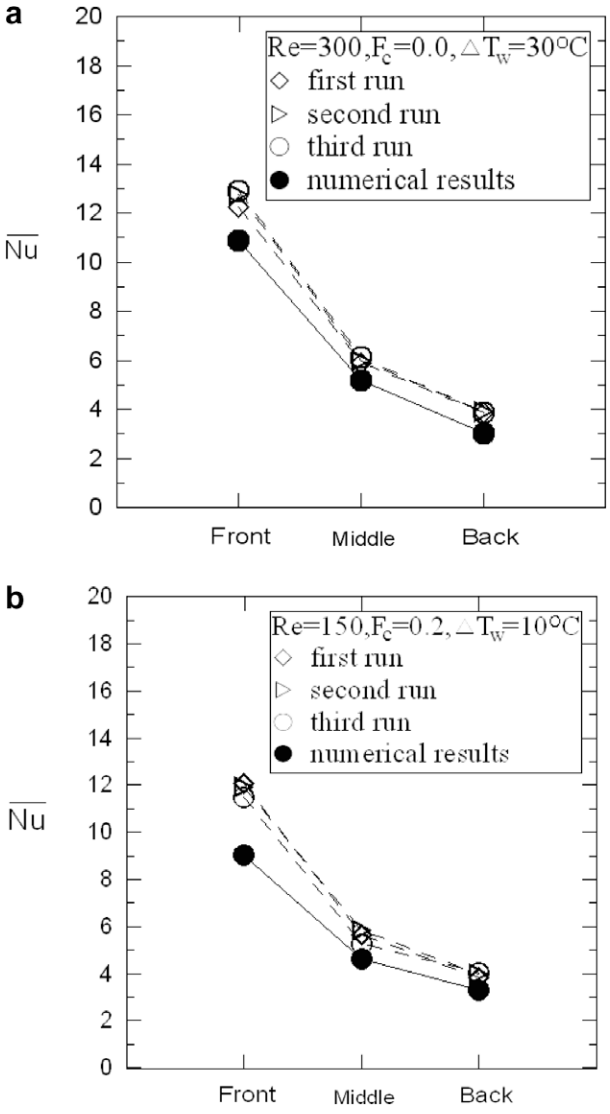

Fig. 5. Validation of reliability of experimental apparatus.

Table 3
Uncertainty analyses of front heat region under $Re = 150$.

Parameters	Dimensions	Uncertainty
w (mm)	30 mm	0.05 (mm)
ΔT_w (°C)	20 °C	±0.3(°C)
L_c	15 mm	±0.11%
Re	300	±3.57%
$\overline{Nu}$	6.04	±5.73%
Gr/Re^2	3.24	±7.29%

Table 4
The maximum reciprocating velocity and mean velocity of inlet fluid.

$v_0(m/s)$	$v_m(m/s)$	
	$F_c = 0.2$	$F_c = 0.4$
$Re = 150$	0.10	0.2
	0.08	0.08
$Re = 200$	0.125	0.25
	0.10	0.10
$Re = 300$	0.20	0.40
	0.16	0.16

of Fig. 6. For the same reason, in the front heat region the magnitude of the average Nusselt number of the larger frequency situation ($F_c = 0.4$) is no longer larger than that of the small frequency situation ($F_c = 0.2$). Similarly, in the back heat region the magnitude of the average Nusselt number of the small frequency ($F_c = 0.2$) is also no longer larger than that of the large frequency situation ($F_c = 0.4$). These above phenomena are different from those in Fig. 6(a) and (c). In the middle heat region, the differences between the Nusselt numbers of the situations of $F_c = 0.2$ and 0.4 are still small which are similar to those indicated in Fig. 6(b).

In Fig. 9, the temperature difference ΔT_w becomes 40 °C, and the magnitude of Gr/Re^2 is equal to 3.64 which is over 1. Except the contribution of forced convection to the heat regions, the effect of natural convection on the heat transfer rates of each heat region increases remarkably. The whole magnitudes of the Nusselt numbers in this situation are larger than those shown in Fig. 8(a)–(c). But the trends of variations of the Nusselt numbers of each heat region are similar to those shown in the above figure.

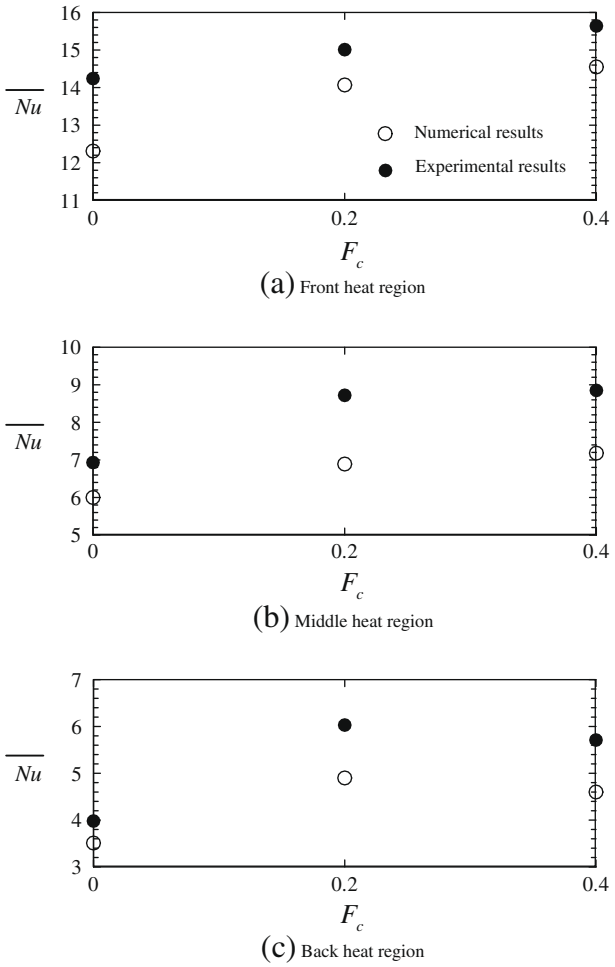

Fig. 6. Distributions of Nusselt numbers under $Re = 300$, $Gr/Re^2 = 0.40$ ($\Delta T_w = 10$ °C), $L_c = 0.5$, $F_c = 0.0$, 0.2, 0.4 situations.

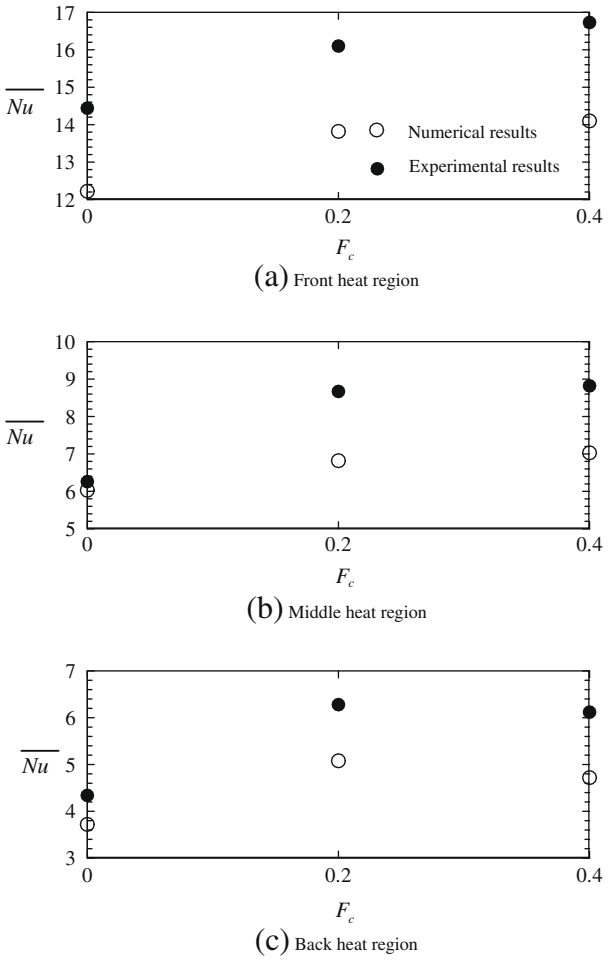

Fig. 7. Distributions of Nusselt numbers under $Re = 300$, $Gr/Re^2 = 1.62$ ($\Delta T_w = 40$ °C), $L_c = 0.5$, $F_c = 0.0$, 0.2, 0.4 situations.

In Fig. 10, the magnitude of the Reynolds number further decreases to 150, which means the influence of the forced convection to become much smaller. Doubtlessly, the magnitudes of the Nusselt numbers indicated in this situation are smaller than those shown in the above two situations (Figs. 6 and 8). Both Nusselt numbers of $F_c = 0.2$ and 0.4 are approximately equivalent in each heat region.

As for the variations of average Nusselt numbers indicated in Fig. 10, because the Reynolds number decreases and equals to 150 which weakens the impulse of the flow. In the middle heat region, the situation of the flow confined completely by the walls of channel is similar to that mentioned in Fig. 6, then the effect of the frequency on the heat transfer rate of the middle heat region is weak. The average Nusselt numbers of the situations of $F_c = 0.2$ and 0.4 are almost equivalent which is like that indicated in Fig. 6(b). When the flow turns round the right corner, the flow can cover the back heat region more completely than that of the larger Reynolds number situation shown in Fig. 6. Also, when the ratio of Gr/Re^2 becomes larger, the effect of the frequency F_c on the heat transfer of the back heat region increases. Consequently, the average Nusselt number of the experimental result of $F_c = 0.4$ situation is almost equal to that of $F_c = 0.2$ situation. The result is somewhat different from that shown in Fig. 6. The experimental trend of the variation of average Nusselt numbers is different from that of numerical results. The model of the computation needs to be modified more carefully in the future.

In Fig. 11, the magnitude of the ratio of Gr/Re^2 is raised and equals to 6.47 which means the effect of natural convection on the heat transfer rates of heat regions to be dominant. The behavior of the frequency can be regarded as a kind of disturbance of which the influence on the natural convection is exceptionally obvious. Therefore, in spite of the confinement of the flow in the middle heat region mentioned above, the enhancement of the average Nusselt number of the $F_c = 0.4$ situation is more effective than that of the $F_c = 0.2$ situation. However, the directions of the natural convection and reciprocating motion are the same and vertical to the direction of the main stream flow. This condition somewhat obstructs the main stream flow and decreases the effect of the forced convection caused by the main stream flow on the heat transfer rate of the middle heat region. As a result, the average Nusselt numbers of the middle heat region of Fig. 11 are smaller than those of Fig. 10 in which the magnitude of the ratio of Gr/Re^2 is small. Also, when the back heat region is close to the right corner, the influence of the confinement of the walls is weak. Then the contributions of the forced and natural convections to the heat transfer rates of the back heat region can be added that is not like the contributions of the both convections to counteract mutually in the middle heat region. And the magnitudes of the average Nusselt numbers of the back heat region indicated in Fig. 11 become larger relative to those indicated in Fig. 10.

In order to estimate the effects of the reciprocating motion on the average Nusselt number of whole heat regions, an enhancement coefficient En is defined as follows and shown in Fig. 12

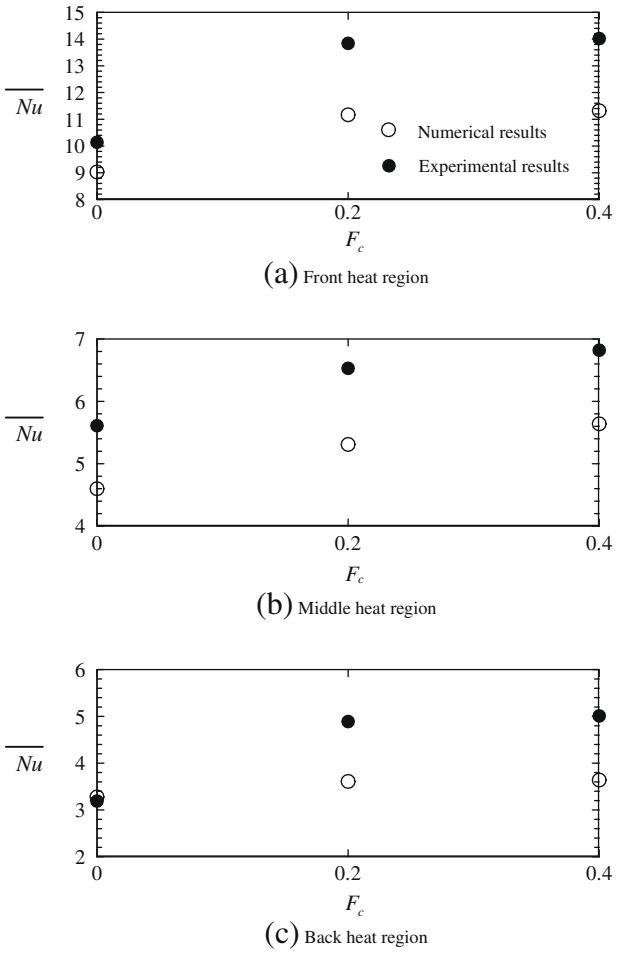

Fig. 8. Distributions of Nusselt numbers under $Re = 200$, $Gr/Re^2 = 0.91$ ($\Delta T_w = 10$ °C), $L_c = 0.5$, $F_c = 0.0, 0.2, 0.4$ situations.

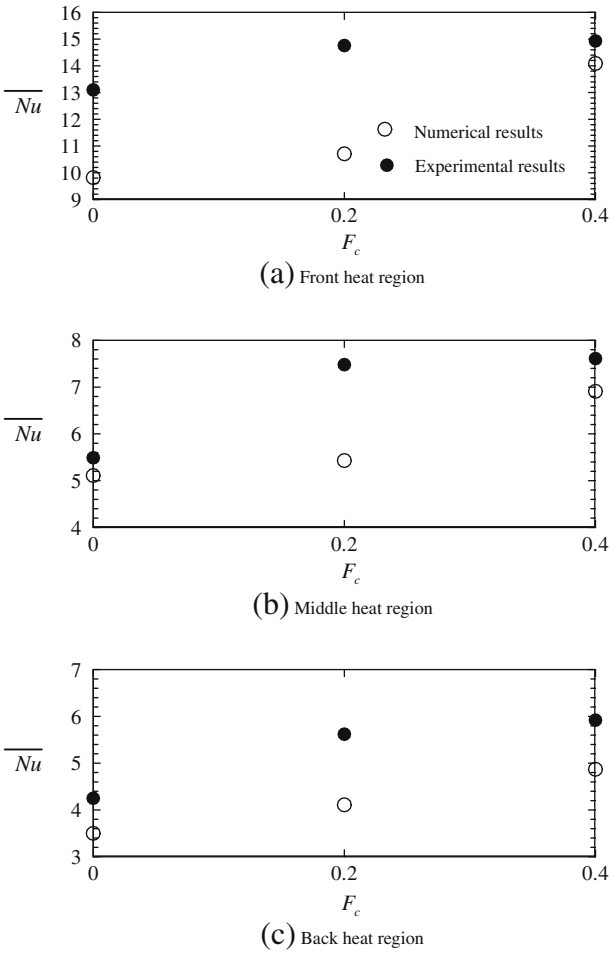

Fig. 9. Distributions of Nusselt numbers under $Re = 200$, $Gr/Re^2 = 3.64$ ($\Delta T_w = 40$ °C), $L_c = 0.5$, $F_c = 0.0, 0.2, 0.4$ situations.

$$\overline{Nu} = \frac{1}{3}\left(\overline{Nu}_{front\ heat\ region} + \overline{Nu}_{middle\ heat\ region} + \overline{Nu}_{back\ heat\ region}\right) \tag{9}$$

$$En = \frac{\overline{Nu}_{F_c, L_c \neq 0} - \overline{Nu}_{F_c, L_c = 0}}{\overline{Nu}_{F_c, L_c = 0}} \tag{10}$$

Generally the enhancement of heat transfer rates of whole heat regions caused by the reciprocating motion is remarkable, and the maximum magnitude of the enhancement coefficient is over 35%. The enhancement coefficients of the situation of the high frequency ($F_c = 0.4$) are universally larger than these of the situation of the low frequency ($F_c = 0.2$). Under the same frequency, due to mutual influence of forced and natural convections the variations of the enhancement coefficients are irregular.

4. Conclusions

Heat transfer phenomena of a ⊔ shape subject to a reciprocating motion are conducted experimentally. The parameters of Reynolds numbers, frequencies are varied and useful results are obtained. Some conclusions are drawn as follows:

1. Due to the influence of impingement phenomenon, the heat transfer rate of the front region is still larger than these of the other two heat regions. Oppositely, the fluid flow has difficulty to flow over the back heat region completely, and the heat transfer rate of the back heat region is always smaller than these of the other two heat regions.
2. Enhancement of heat transfer rate by a reciprocating motion is definitely effective in spite of under any convection modes. However, the relationships between frequency and convection heat transfer mode should be considered simultaneously.

Acknowledgement

The support of this study by the National Science Council of Taiwan, ROC, under Contact NSC97-2221-E-009-144-MY2 is gratefully acknowledged.

Appendix A. The analysis of uncertainty for Nusselt number (for $Re = 300$, $Gr/Re^2 = 0.81$, $\Delta T_w = 20$ °C, $F_c = 0.2$)

The Nusselt number is expressed as $\overline{Nu} = \frac{Q_{air}}{A_h \Delta T_w} \cdot \frac{w}{k}$, and the uncertainty for $\overline{Nu}$ is estimated as follows:

$$\frac{\delta \overline{Nu}}{\overline{Nu}} = \left[\left(\frac{\delta Q_{air}}{Q_{air}}\right)^2 + \left(\frac{\delta w}{w}\right)^2 + \left(-\frac{\delta A_h}{A_h}\right)^2 + \left(-\frac{\delta \Delta T_w}{\Delta T_w}\right)^2 + \left(-\frac{\delta k_a}{k_a}\right)^2\right]^{1/2} \tag{A.1}$$

A.1. The uncertainty for heat energy dissipated by a mixed convection

Q_{air} is the heat energy dissipated by a mixed convection, and can be expressed as the following equation:

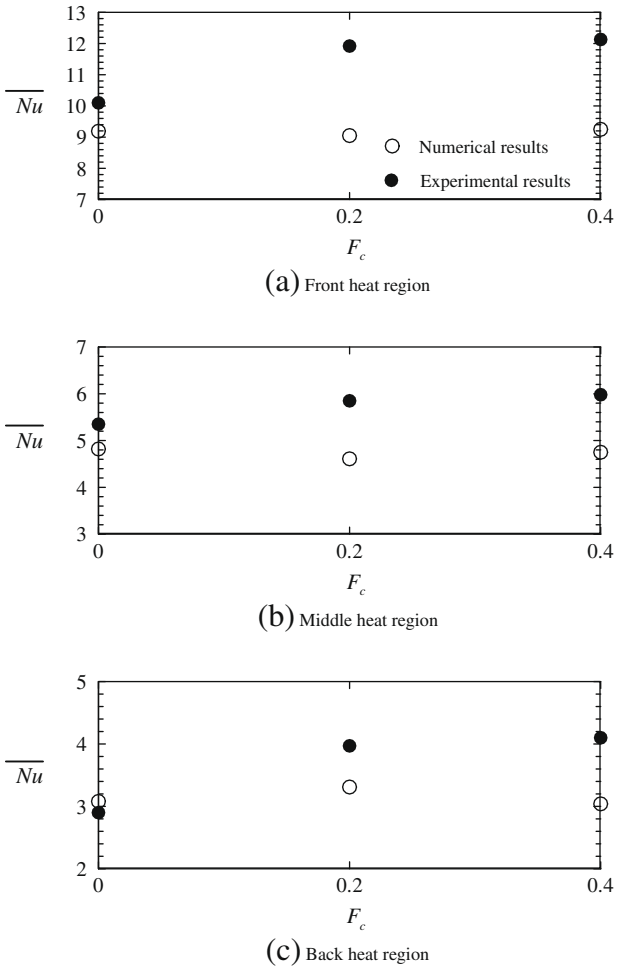

Fig. 10. Distributions of Nusselt numbers under $Re = 150$, $Gr/Re^2 = 1.62$ ($\Delta T_w = 10$ °C), $L_c = 0.5$, $F_c = 0.0$, 0.2, 0.4 situations.

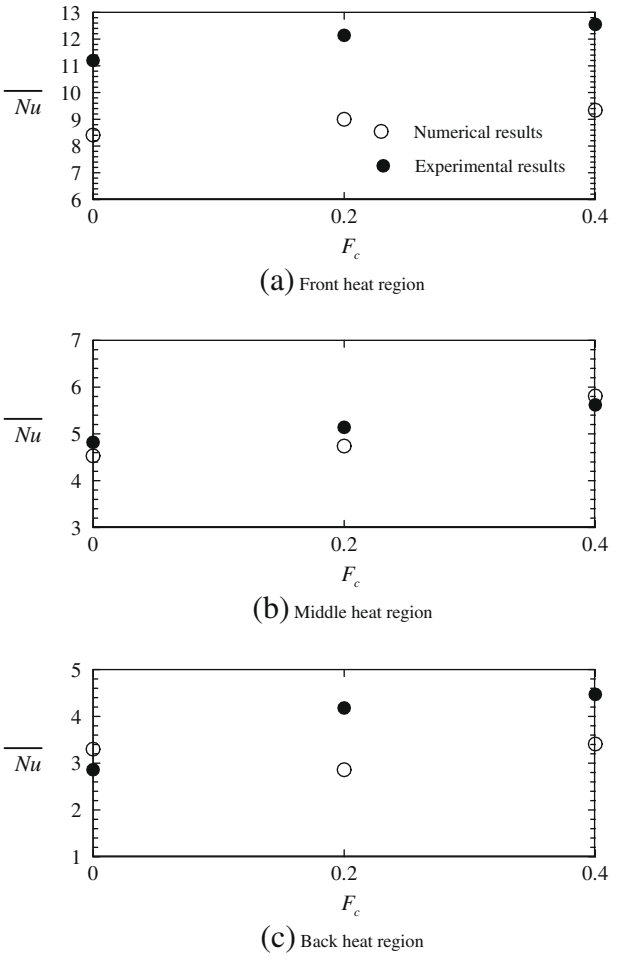

Fig. 11. Distributions of Nusselt numbers under $Re = 150$, $Gr/Re^2 = 6.47$ ($\Delta T_w = 40$ °C), $L_c = 0.5$, $F_c = 0.0$, 0.2, 0.4 situations.

$$Q_{air} = Q_{in} - Q_{loss} - Q_{712\to711} - Q_{712\to713} - Q_{712\to714} - Q_{712\to715} = 0.181 \quad (\mathrm{W}) \tag{A.2}$$

And the uncertainty for Q_{air} is

$$\frac{\delta Q_{air}}{Q_{air}} = \left[\left(\frac{Q_{in}}{Q_{air}}\frac{\delta Q_{in}}{Q_{in}}\right)^2 + \left(\frac{Q_{loss}}{Q_{air}}\frac{\delta Q_{loss}}{Q_{loss}}\right)^2 + \left(\frac{Q_{712\to711}}{Q_{air}}\frac{\delta Q_{712\to711}}{Q_{712\to711}}\right)^2 + \left(\frac{Q_{712\to713}}{Q_{air}}\frac{\delta Q_{712\to713}}{Q_{712\to713}}\right)^2 + \left(\frac{Q_{712\to714}}{Q_{air}}\frac{\delta Q_{712\to714}}{Q_{712\to714}}\right)^2 + \left(\frac{Q_{712\to715}}{Q_{air}}\frac{\delta Q_{712\to715}}{Q_{712\to715}}\right)^2\right]^{1/2} \tag{A.3}$$

A. The uncertainty for input heat energy

The input heat energy is

$$Q_{in} = V \times I = 2.5 \times 0.127 = 0.3175 \quad (\mathrm{W}) \tag{A.4}$$

The minimum sensitivities of the multimeters for voltage and current probing are 0.001 V and 0.001 A, respectively. Then the uncertainty for input heat energy can be calculated as following equation:

$$\frac{\delta Q_{in}}{Q_{in}} = \left[\left(\frac{\delta V}{V}\right)^2 + \left(\frac{\delta I}{I}\right)^2\right]^{1/2} = \left[\left(\frac{0.0005}{2.5}\right)^2 + \left(\frac{0.0005}{0.127}\right)^2\right]^{1/2} = 0.39\% \tag{A.5}$$

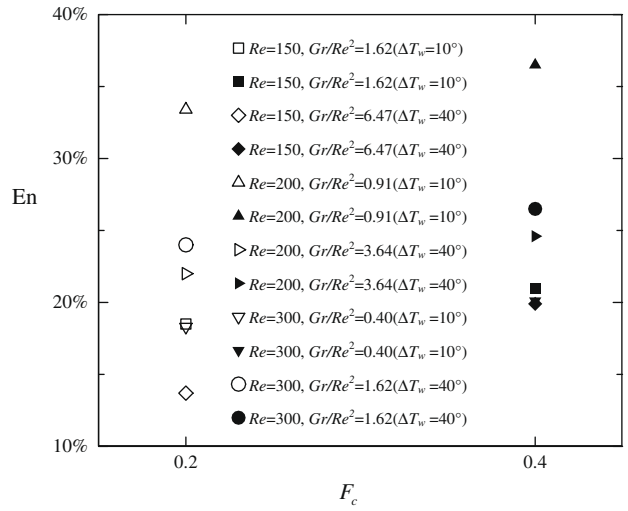

Fig. 12. Effects of a reciprocating motion on heat transfer rates.

B. The uncertainty for heat energy dissipated by heat conduction mode.

From the equation of heat conduction $Q_{lose} = k_b \times A_b \times dT/dy$, the uncertainty for heat energy dissipated by heat conduction mode can be expressed as

$$\frac{\delta Q_{lose}}{Q_{lose}} = \left[\left(\frac{\delta k_b}{k_b}\right)^2 + \left(\frac{\delta A_b}{A_b}\right)^2 + \left(\frac{\delta dT}{dT}\right)^2 + \left(-\frac{\delta dy}{dy}\right)^2\right]^{1/2} \quad (A.6)$$

where k_b and A_b are the conductivity and area of the balsawood, respectively.

(1) The conductivity of the balsawood is estimated from the table of physical prosperities of material, therefore the uncertainty for conductivity of the balsawood is approached to 0.

(2) The dimensions of the balsawood are 62.00 by 12.00 mm and the minimum grid of the vernier caliper is 0.05 mm. The uncertainty for the area of the balsawood is

$$\frac{\delta A_b}{A_b} = \left[\left(\frac{0.025}{62.00}\right)^2 + \left(\frac{0.025}{12.00}\right)^2\right]^{1/2} = 0.21\% \quad (A.7)$$

(3) The maximum temperature difference in experiments is 45.7–43.8 = 1.9 °C and the measuring accuracy of DA2500E is 0.1 °C. Therefore, the uncertainty for temperature difference is expressed as the following equation:

$$\frac{\delta dT}{dT} = \left[\left(\frac{0.05}{1.9}\right)^2\right]^{1/2} = 2.63\% \quad (A.8)$$

(4) The thickness of balsawood is 1.5 mm and the minimum grid of the vernier caliper is 0.05 mm. The uncertainty for the thickness of balsawood is

$$\frac{\delta dy}{dy} = \left[\left(\frac{0.025}{1.5}\right)^2\right]^{1/2} = 1.66\% \quad (A.9)$$

According to the above derivations, the uncertainty for heat energy dissipated by heat conduction mode is calculated as follows:

$$\frac{\delta Q_{lose}}{Q_{lose}} = [(0)^2 + (0.21\%)^2 + (2.63\%)^2 + (-1.66\%)^2]^{1/2} = 3.12\% \quad (A.10)$$

C. The uncertainty for the heat transfer between heaters (711) and (712)

From the heat conduction equation, $Q_{742\to741} = k_m \times A_m \times dT/dx$, the uncertainty for the heat transfer between heater 1 and heater 2 can be written as

$$\frac{\delta Q_{712\to711}}{Q_{712\to711}} = \left[\left(\frac{\delta k_m}{k_m}\right)^2 + \left(\frac{\delta A_m}{A_m}\right)^2 + \left(\frac{\delta dT}{dT}\right)^2 + \left(-\frac{\delta dx}{dx}\right)^2\right]^{1/2} \quad (A.11)$$

where k_m and A_m are the conductivity of thermal conductive adhesive and the contacting area of two heaters.

(1) The conductivity of thermal conductive adhesive, OB200, is obtained from user manual, therefore the uncertainty is approaching to 0.

(2) The contacting area of two heaters is 62.00 by 2.00 mm, and the minimum grid of the vernier caliper is 0.05 mm. Thus, the uncertainty for contacting area is

$$\frac{\delta A_m}{A_m} = \left[\left(\frac{0.025}{62.00}\right)^2 + \left(\frac{0.025}{2}\right)^2\right]^{1/2} = 1.25\% \quad (A.12)$$

(3) The temperature difference between two heaters is regarded as isothermal condition, and then the uncertainty for temperature difference dT is 0.

(4) The thickness of thermal conductive adhesive is 1.5 mm, and the minimum grid of the vernier caliper is 0.05 mm. The uncertainty for thickness of thermal conductive adhesive is written as

$$\frac{\delta dx}{dx} = \left[\left(\frac{0.025}{1.5}\right)^2\right]^{1/2} = 1.67\% \quad (A.13)$$

From the above derivations, the uncertainty for the heat transfer between heater 711 and heater 712 is written as following equation:

$$\frac{\delta Q_{712\to711}}{Q_{712\to711}} = [(0)^2 + (1.25\%)^2 + (0)^2 + (-1.67\%)^2]^{1/2} = 2.08\% \quad (A.14)$$

D. Similarly, the uncertainties for the heat transfer between the heaters (712) and (713), (712) and (714), (712) and (715) are 2.08%, 2.1%, 2.1%, respectively.

A.2. The uncertainty for the width of reciprocating channel

The width of ⊔ shape channel is 29.90 mm, and the minimum grid of the vernier caliper is 0.05 mm. The uncertainty for the width of testing channel is written as following equation:

$$\frac{\delta w}{w} = \left[\left(\frac{0.025}{29.90}\right)^2\right]^{1/2} = 0.08\% \quad (A.15)$$

A.3. The uncertainty for the area of heaters

The area of heaters is 62.00 by 12.00 mm, and the minimum grid of the vernier caliper is 0.05 mm. Then the uncertainty for the area of heaters can be written as

$$\frac{\delta A_h}{A_h} = \left[\left(\frac{0.025}{62.00}\right)^2 + \left(\frac{0.025}{12.00}\right)^2\right]^{1/2} = 0.21\% \quad (A.16)$$

A.4. The uncertainty for temperature difference between heaters and environment

The maximum temperature difference is 19.9 °C, and the accuracy of DA2500E is 0.1 °C. The temperature difference less than 0.3 °C is regarded as isothermal condition, and then the uncertainty for temperature difference between heaters and environment is written as

$$\frac{\delta \Delta T_w}{\Delta T_w} = \left[\left(\frac{0.3}{19.9}\right)^2\right]^{1/2} = 1.51\% \quad (A.17)$$

A.5. The uncertainty for conductivity of working fluid

The conductivity of working fluid, air, is known from material chart, then the uncertainty for conductivity of working fluid is approaching 0.

Substituting the above derivations into Eq. (A.1), the uncertainty for $\overline{Nu}$ is then estimated as following equation:

$$\begin{aligned}\frac{\delta \overline{Nu}}{\overline{Nu}} &= \left[\left(\frac{\delta Q_{air}}{Q_{air}}\right)^2 + \left(\frac{\delta w}{w}\right)^2 + \left(-\frac{\delta A_h}{A_h}\right)^2 + \left(-\frac{\delta \Delta T_w}{\Delta T_w}\right)^2 + \left(-\frac{\delta k_a}{k_a}\right)^2\right]^{1/2} \\ &= [(1.12\%)^2 + (0.08\%)^2 + (-0.21\%)^2 + (-1.51\%)^2 + (0\%)^2]^{1/2} \\ &= 1.89\%\end{aligned} \quad (A.18)$$

Appendix B. The analysis of uncertainty for Reynolds number

The Reynolds number is expressed as $Re = \frac{v_0 \cdot w}{\upsilon}$, then the uncertainty for Reynolds number can be written as following equation:

$$\frac{\delta Re}{Re} = \left[\left(\frac{\delta v_0}{v_0}\right)^2 + \left(\frac{\delta w}{w}\right)^2 + \left(-\frac{\delta \upsilon}{\upsilon}\right)^2\right]^{1/2} \tag{A.19}$$

B.1. The uncertainty for inlet velocity of working fluid

The inlet velocity is estimated by equation $v_0 = \frac{\dot{Q}}{A} = \frac{\dot{Q}}{w \cdot z}$, where A is the cross-section area of the channel and z is the height of the channel. According to the uncertainty equation, the uncertainty for inlet velocity of working fluid can be estimated as following equation:

$$\frac{\delta v_0}{v_0} = \left[\left(\frac{\delta \dot{Q}}{\dot{Q}}\right)^2 + \left(-\frac{\delta w}{w}\right)^2 + \left(-\frac{\delta z}{z}\right)^2\right]^{1/2} \tag{A.20}$$

$\dot{Q}$ is the volume flow rate measured by a flow meter, and the accuracy is 20 cc/s. w and z are 29.90 mm and 120.7 mm, respectively. Then Eq. (A.20) can be written as

$$\frac{\delta v_0}{v_0} = \left[\left(\frac{10}{560}\right)^2 + \left(-\frac{0.025}{29.90}\right)^2 + \left(-\frac{0.025}{120.7}\right)^2\right]^{1/2} = 1.78\% \tag{A.21}$$

B.2. The uncertainty for the width of channel

The width of channel is 29.90 mm, and the minimum grid of the vernier caliper is 0.05 mm. The uncertainty for the width of testing channel is written as following equation:

$$\frac{\delta w}{w} = \left[\left(\frac{0.025}{29.90}\right)^2\right]^{1/2} = 0.08\% \tag{A.22}$$

B.3. The uncertainty for kinetic viscosity of working fluid

The kinetic viscosity of working fluid, air, is known from material chart, then the uncertainty for kinetic viscosity of working fluid is approaching to 0.

Substituting the above derivations into Eq. (A.19), the uncertainty for Re is then estimated as follows:

$$\frac{\delta Re}{Re} = [(1.78\%)^2 + (0.08\%)^2 + (0\%)^2]^{1/2} = 1.78\% \tag{A.23}$$

Appendix C. The analysis of uncertainty for non-dimensional reciprocating amplitude

The non-dimensional reciprocating amplitude is written as $L_c = l_c/w$, then the uncertainty for non-dimensional amplitude can be expressed as following equation:

$$\frac{\delta L_c}{L_c} = \left[\left(\frac{\delta l_c}{l_c}\right)^2 + \left(-\frac{\delta w}{w}\right)^2\right]^{1/2} \tag{A.24}$$

The reciprocating amplitude l_c is 30.5 mm, and the minimum grid of the vernier caliper is 0.05 mm

$$\frac{\delta l_c}{l_c} = \left[\left(\frac{0.025}{30.5}\right)^2\right]^{1/2} = 0.08\% \tag{A.25}$$

From equations mentioned above, the uncertainty for width of channel is 0.08%. Then the uncertainty for non-dimensional reciprocating amplitude can be estimated as following equation:

$$\frac{\delta L_c}{L_c} = [(0.08\%)^2 + (-0.08\%)^2]^{1/2} = 0.11\% \tag{A.26}$$

Appendix D. The analysis of uncertainty for non-dimensional reciprocating frequency

The non-dimensional reciprocating frequency is written as $F_c = f_c \cdot w/v_0$, then the uncertainty for non-dimensional frequency can be expressed as following equation:

$$\frac{\delta F_c}{F_c} = \left[\left(\frac{\delta f_c}{f_c}\right)^2 + \left(\frac{\delta w}{w}\right)^2 + \left(-\frac{\delta v_o}{v_o}\right)^2\right]^{1/2} \tag{A.27}$$

It is taken 120 s for the channel to reciprocate 120 times, and the minimum time interval for the timer is 0.1 s. Therefore the uncertainty for reciprocating frequency is as follows:

$$\frac{\delta f_c}{f_c} = \left[\left(\frac{0.05}{120}\right)^2\right]^{1/2} = 0.04\% \tag{A.28}$$

The uncertainties for the width of channel and inlet velocity of working fluid are mentioned above. Then the uncertainty for Reynolds number is estimated as follows:

$$\frac{\delta F_c}{F_c} = [(0.04\%)^2 + (0.08\%)^2 + (-1.79\%)^2]^{1/2} = 1.79\% \tag{A.29}$$

Appendix E. The analysis of uncertainty for Gr/Re^2

The uncertainty for Gr/Re^2 is expressed as following equation:

$$\frac{\delta(Gr/Re^2)}{(Gr/Re^2)} = \left[\left(\frac{\delta g}{g}\right)^2 + \left(\frac{\delta \beta}{\beta}\right)^2 + \left(\frac{\delta \Delta T_w}{T_w}\right)^2 + \left(\frac{\delta w}{w}\right)^2 + \left((-2)\times\frac{\delta v_o}{v_o}\right)^2\right]^{1/2} \tag{A.30}$$

The earth gravity and expansion coefficient are both known from material chart, therefore the uncertainties are limited to 0. The uncertainties for the temperature difference, width of channel and inlet velocity of working fluid are mentioned above, and are 1.5%, 0.08% and 1.79%, respectively. Then the Eq. (A.30) can be estimated as follows:

$$\begin{aligned}\frac{\delta(Gr/Re^2)}{(Gr/Re^2)} &= \left[\left(\frac{\delta g}{g}\right)^2 + \left(\frac{\delta \beta}{\beta}\right)^2 + \left(\frac{\delta \Delta T_w}{T_w}\right)^2 + \left(\frac{\delta w}{w}\right)^2 + \left((-2)\times\frac{\delta v_o}{v_o}\right)^2\right]^{1/2} \\ &= [(0)^2 + (0)^2 + (1.5\%)^2 + (0.08\%)^2 + ((-2)\times 1.79\%)^2]^{1/2} = 3.88\%\end{aligned} \tag{A.31}$$

References

[1] S.W. Chang, L.M. Su, Heat transfer a reciprocating duct fitted with transverse ribs, Exp. Heat Transfer 12 (1999) 95–115.

[2] P.P. Grassmann, M. Tuma, Applications of the electrolytic method-II. Mass transfer within a tube for steady, oscillating and pulsating flows, Int. J. Heat Mass Transfer 22 (1979) 799–804.

[3] A.T. Patera, B.B. Mikic, Exploiting hydrodynamic instabilities resonant heat transfer enhancement, Int. J. Heat Mass Transfer 29 (8) (1986) 1127–1138.

[4] S.Y. Kim, B.H. Kang, A.E. Hyun, Heat transfer in the thermally developing region of a pulsating channel flow, Int. J. Heat Mass Transfer 36 (17) (1993) 1257–1266.

[5] T. Nishimura, N. Kojima, Mass transfer enhancement in a symmetric sinusoidal wavy-walled channel for pulsatile flow, Int. J. Heat Mass Transfer 38 (9) (1995) 1719–1731.

[6] T. Nishimura, A. Taurmoto, Y. Kawamura, Flow and mass transfer characteristics in wavy channels for oscillatory flow, Int. J. Heat Mass Transfer 38 (1987) 1007–1015.
[7] T. Nishimura, S. Arakawa, D. Murakami, Y. Kawamura, Oscillatory flow in a symmetric sinusoidal wavy-walled channel at intermediate Strouhal numbers, Chem. Eng. Sci. 46 (1991) 757–771.
[8] T. Nishimura, S. Arakawa, D. Murakami, Y. Kawamura, Oscillatory viscous flow in symmetric sinusoidal wavy-walled channels, Chem. Eng. Sci. 44 (1989) 2137–2148.
[9] C.P. Chiu, Y.S. Kuo, Study of turbulent heat transfer in reciprocating engine using as algebraic grid generation technique, Numer. Heat Transfer A 27 (1995) 255–271.
[10] S.W. Chang, L.M. Su, Influence of reciprocating motion on heat transfer inside a ribbed duct with application to piston cooling in marine diesel engines, J. Ship Res. 41 (4) (1997) 332–339.
[11] C.H. Cheng, C.K. Hung, Numerical predictions of flow thermal fields in a reciprocating piston–cylinder assembly, Numer. Heat Transfer A 38 (2000) 397–421.
[12] C. Sert, A. Beskok, Oscillatory flow forced convection in micro heat spreaders, Numer. Heat Transfer A 42 (2002) 685–705.
[13] A.R.A. Khaled, K. Vafai, Heat transfer and hydromagnetic control of flow exit conditions inside oscillatory squeezed thin films, Numer. Heat Transfer A 43 (2003) 239–258.
[14] S.W. Chang, L.M. Su, W.D. Morris, T.M. Liou, Heat transfer in a smooth-walled reciprocating anti-gravity open thermosyphon, Int. J. Heat Mass Transfer 42 (2003) 1089–1103.
[15] W.S. Fu, S.H. Lian, Y.H. Liao, An investigation of heat transfer of a reciprocating piston, Int. J. Heat Mass Transfer 49 (2006) 4360–4371.
[16] S.W. Chang, L.M. Su, T.L. Yang, S.F. Chiou, Enhanced heat transfer of shaker-bored piston cooling channel with twisted tape insert, Heat Transfer Eng. 28 (4) (2007) 321–334.
[17] S.W. Chang, W.D. Morris, T.M. Liou, S.F. Chiou, Heat transfer in a reciprocating thermosyphon fitted with staggered transverse ribs, J. Thermophys. Heat Transfer 21 (3) (2007) 568–581.
[18] W.S. Fu, W.J. Shieh, A study of thermal convection in an enclosure induced simultaneously by gravity and vibration, Int. J. Heat Mass Transfer 35 (1992) 1695–1710.
[19] W.S. Fu, W.J. Shieh, Transient thermal convection in an enclosure induced simultaneously by gravity and vibration, Int. J. Heat Mass Transfer 36 (1992) 437–452.
[20] G.Z. Gershuni, D.V. Lyubimov, Thermal Vibrational Convection, John Wiley and Sons, New York, 1998.
[21] Wärtsilä. Available from: <http://www.wartsila.com/>.
[22] S.J. Kline, The purpose of uncertainty analysis, ASME J. Heat Transfer 117 (1985) 153–160.